Correspondence to:
J. S. McNeal,
mcneal@pdx.edu

Investigating the Accuracy of One-Dimensional Volcanic Plume Models using Laboratory Experiments and Field Data

James S. McNeal[1,2] [ID], **Graham Freedland[2]**, **Larry G. Mastin[3]** [ID], **Raúl Bayoán Cal[2]**, and **Stephen A. Solovitz[1]**

[1]School of Engineering and Computer Science, Washington State University Vancouver, Vancouver, WA, USA, [2]Maseeh College of Engineering, Portland State University, Portland, OR, USA, [3]Cascades Volcano Observatory, U.S. Geological Survey, Vancouver, WA, USA

Abstract During volcanic eruptions, model predictions of plume height are limited by the accuracy of entrainment coefficients used in many plume models. Typically, two parameters are used, α and β, which relate the entrained air speed to the jet speed in the axial and cross-flow directions, respectively. To improve estimates of these parameters, wind tunnel experiments have been conducted for a range of cross-wind velocities and turbulence conditions. Measurements are compared directly to computations from the 1-D plume model, Plumeria, in the near-field, bending region of the jet. Entrainment coefficients are determined through regression analysis, demonstrating optimal combinations of effective α and β values. For turbulent conditions, all wind speeds overlapped at a single combination, $\alpha = 0.06$ and $\beta = 0.46$, each of which are slightly reduced from standard values. Refined coefficients were used to model plume heights for 20 historical eruptions. Model accuracy improves modestly in most cases, agreeing to within 3 km with observed plume heights. For weak eruptions, uncertainty in field measurements can outweigh the effects of these refinements, illustrating the challenge of applying plume models in practice.

1. Introduction

Volcanic eruptions are inherently dangerous to human life and activity. The type of eruption determines the area at risk during a volcanic eruption, where the largest affected areas are associated with explosive eruptions involving buoyant volcanic columns. Eruptions like Eyjafjallajökull in Iceland (2010), Etna in Italy (2002), Kelud in Indonesia (2014), and Kilauea in Hawaii (2018) bring the dangers to the forefront of scientific attention and highlight the need for predictive and preventative measures. In particular, the 2010 eruption of Eyjafjallajökull resulted in a public policy shift that heightened the need for accurate models of plume behavior (Bonadonna et al., 2012).

Ash transport models (ATMs) forecast the path and concentrations of volcanic ash clouds and are used to assign areas to avoid by aircraft. A critical source parameter for all ATMs is mass eruption rate (MER) as MER affects ATM estimations of airborne particle concentrations and fallout. MER is estimated either through field observations or mathematical plume models. One-dimensional steady-state numerical plume models, for example, Plumeria, are commonly used to estimate *MER* through inversion of observed plume height (H_{obs}). In practice, forecasters input weather conditions and H_{obs} that allow for real-time *MER* estimates used in ATM models for hazard assessments. These models can be used in real time, making them possible tools for operations. There are several models available (Costa et al., 2016), all of which operate along the same physical principles of mass, momentum, and energy conservation. Despite their utility and flexibility, 1-D plume model accuracy is limited by model parameters and field data uncertainty.

Although based on fundamental concepts, 1-D plume models require the use of empirical parameters related to entrainment. Hence, their accuracy is limited by the understanding of entrainment (Costa et al., 2016; Woodhouse et al., 2015), which this research aims to address. For plumes in cross flow, two parameters are used to describe entrainment: α and β. The former parameter quantifies entrainment associated with shear due to differential flow velocities parallel to the axis of the plume, while the latter is associated with entrainment due to shear perpendicular to the axis of the plume (i.e., cross flow). The entrainment coefficients are

Table 1
Inflow and Jet Velocities and Corresponding Ratios for Passive and Active Grid Experiments

Passive grid ($TI \sim 5\%$)			Active grid ($TI \sim 10 - 15\%$)		
u_{wind} (m/s)	u_{jet} (m/s)	R_v (R_v^{-1})	u_{wind} (m/s)	u_{jet} (m/s)	R_v (R_v^{-1})
2.97	40.3	13.6 (0.074)	1.97	41.5	21 (0.048)
3.87	40.7	10.5 (0.095)	2.39	40.7	17.1 (0.058)
4.78	39.6	8.28 (0.121)	2.80	41.2	14.7 (0.068)
5.69	40.7	7.15 (0.140)	3.21	40.7	12.7 (0.079)
6.60	41.1	6.23 (0.161)	4.03	41.5	10.3 (0.097)
			4.85	41.3	8.5 (0.118)

Note. All data were taken from Freedland (2016). Jet-to-wind velocity ratio provided in alternative format ($R_v^{-1} = u_{wind}/u_{jet}$). The jet ejecta was compressed air.

based on velocity ratios between the local plume centerline velocity u_{jet} and the parallel and normal components of the cross wind (v), $v_\parallel$, and $v_\perp$, respectively. Even though the basic framework for this methodology is well established (Morton et al., 1956; Briggs, 1965), there are significant differences in the entrainment coefficient values between 1-D plume models. This can have a large impact on ash transport estimates, as a doubling of the entrainment coefficient may lead to a fourfold increase in estimates of *MER* (Solovitz & Mastin, 2009).

Of the two empirical coefficients, the axial value, α, ($\alpha = v_\parallel/u_{jet}$; see section 2.3) is better constrained. For fully developed jets and plumes, α is found to vary in both analog experiments (e.g., Kaminski et al., 2005) and 3D multiphase models (e.g., Suzuki & Koyaguchi, 2012; Suzuki & Koyaguchi, 2015). However, α is commonly treated as a constant (Pope, 2000), as demonstrated in classic experiments (e.g., Agrawal & Prasad, 2003; Fischer et al., 1979; Hussein et al., 1994). For momentum-driven jets, measured values of α are close to 0.06 (Agrawal & Prasad, 2003; Fischer et al., 1979), while plumes have magnitudes near 0.09 (e.g., Baines, 1983; Turner, 1986; Woods & Caulfield, 1992) although some 3-D plume models suggest even lower values (e.g., 0.05; Suzuki & Koyaguchi, 2015). Entrainment depends on a variety of other properties, such as axial position (Falcone & Cataldo, 2003) and Reynolds number (Ricou & Spalding, 1961), but α remains between 0.05 to 0.15. Hence, most models choose α values between 0.08 (e.g., Briggs, 1965) and 0.15 (e.g., Bursik, 2001)

The cross-flow coefficient, β, ($\beta = v_\perp/u_{jet}$; see section 2.3) varies over a larger range, partly due to its definition. This parameter is most appropriate for strongly bent-over plumes, where the flow can be modeled as self-similar, allowing β to be treated as a constant. Most plumes in cross flow involve a bending region that is neither wholly vertical nor horizontal, yet most models still select a constant β due to its simplicity. Laboratory measurements suggest β values near 0.6 (e.g., Hewett et al., 1971; Hoult et al., 1969; Huq & Stewart, 1996), yet these same studies applied different values in comparison to field tests, with $\beta \sim 0.4$ to 0.9. These deviations partly occurred due to the laboratory test conditions, which usually considered uniform, low-turbulence cross-wind conditions that differed from the atmosphere. While some studies have used 1D models for β that vary with flow conditions (e.g., Briggs, 1984), constant β values used in 1-D plume models range from approximately 0.1 (Suzuki & Koyaguchi, 2015) to near unity (e.g., Bursik, 2001; Woodhouse et al., 2013). Further, 1-D steady-state models that use a constant β value better predict plume height than models that vary β with Richardson number (Aubry et al., 2017). Many models incorporate a cross-wind entrainment coefficient around $\beta = 0.5$. (e.g., Bonadonna et al., 2012; Costa et al., 2016; Degruyter & Bonadonna, 2012; Devenish et al., 2010). Given that small variations in β have a large impact on estimations of *MER*, entrainment coefficient accuracy is an ongoing concern in both plume models and ATMs.

A primary goal of this work is to evaluate α and β values and accuracy used in 1-D plume models. To that end, a three-step approach was taken that connects the laboratory results to eruption data taken in the field. First, experiments were performed using particle image velocimetry (PIV) of a jet in a wind tunnel at several jet-to-cross wind velocities, expanding on recent high-resolution experiments of similar geometries (Karagozian, 2014; Su & Mungal, 2004). Experiment conditions incorporated a variety of wind conditions (Table 1), as well as variations in free stream turbulence. The data were analyzed to extract the jet centerline, analogous to the output of the 1-D plume model, Plumeria (Mastin, 2007, 2014).
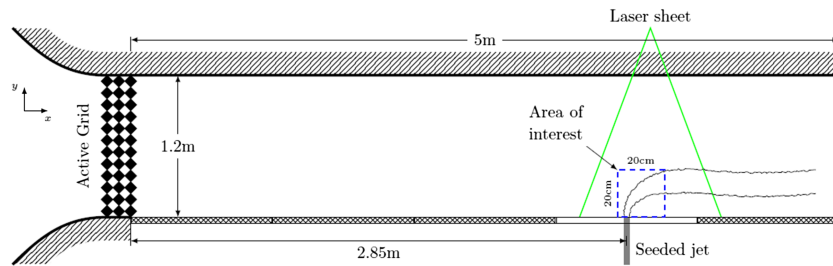
Figure 1. Test section of wind tunnel at PSU (Freedland, 2016). *Not to scale.*

Second, iterations of Plumeria were conducted using the known experimental source and environment parameters as input and boundary conditions. Plumeria incremented α and β values until best fits were found for experiment jet trajectories. The output centerlines were compared to the experimental centerlines using statistical regression methods. The results of the analysis revealed insights into the relationships between the two entrainment coefficients, showing higher model sensitivity to the β value. A pseudolinear α-β trend is seen in best fit cases.

Third, 20 historical eruption were tested to verify if the α and β value modifications from the second step improved predictions of volcanic plume behavior. Plumeria iterations were performed, and the output plume height estimates were compared against historical data. This method showed improved estimates for some eruptions yet demonstrated limitations due to information related to historical eruption data. A more focused study of webcam footage from Eyjafjallajökull provided an alternate means to assess the impact of refined entrainment coefficients.

2. Experimental Methods

Wind tunnel experiments were performed at Portland State University, measuring near-field velocity fields of a jet in a cross wind. Figure 1 shows a schematic of the 0.8 m × 1.2 m test section. The facility and experiments are described in detail by Freedland (2016) and summarized here. This is a closed-circuit wind tunnel featuring an active grid composed of rotating arrays of diamond-shaped winglets that generate turbulence when activated. The seeded jet (diameter $d = 9.525$ mm) is compressed air seeded with micron-scale oil droplets injected perpendicular to the ambient flow field (x direction). Seeded oil droplets allow PIV tracking of the flow field. Tunnel flow speeds , u_{wind}, are adjusted over a range of 2–20 m/s. Because the working fluid of both the jet and cross flow was air of similar temperature, variations in density are regarded as trivial and were not considered in this study. For this discussion, passive grid refers to cases when the winglets were not activated, with turbulence intensities of ~5%. Active grid refers to cases where the winglets were activated, resulting in turbulence intensities of ~10–15%.

Near-exit flow field velocity measurements were taken via stereoscopic PIV (SPIV) technology. The technique provides 2D3C PIV, using two offset cameras to collect three components of velocity within a two-dimensional plane. The lab setup features a Nd:YAG (532 nm, 1,200 mJ, and 4 ns duration) double-pulsed laser and two 4-MP charge-coupled device cameras (frame rate: 4 Hz). The system is controlled by commercial processing software, measuring a square cross-sectional window bisecting the jet with an edge length of approximately 20 cm (pixel edge length: ~0.8 mm).

2.1. Test Conditions

A variety of cross-wind flow velocities were tested for both passive and active grid turbulence intensities. To facilitate cross comparisons, the jet-to-cross wind velocity ratio of Hoult et al. (1969) was used,

$$R_v = u_{jet}/u_{wind} \tag{1}$$

Flow speed regimes were $6.23 < R_v < 13.6$ ($0.074 < R_v^{-1} < 0.161$) for passive grid cases and $8.5 < R_v < 21$ ($0.048 < R_v^{-1} < 0.118$) for active grid cases (Table 1). Because of the nature of the measurements and the presence of varying levels of cross-wind turbulence in the test section, mean convergence required large image sample sizes. For passive grid cases, 2,500 SPIV image sets were captured. For active grid cases, 3,000 SPIV image sets were captured. For each test condition, the mean flow statistics were computed. The streamwise
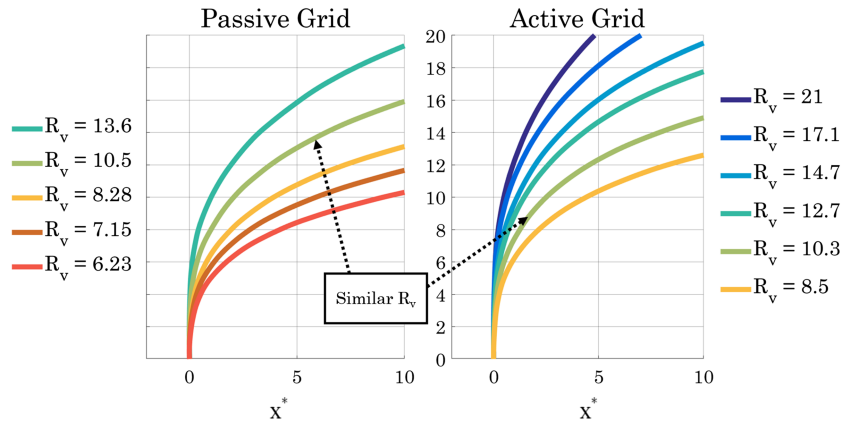
Figure 2. Processed experimental streamlines extracted from SPIV data.

and vertical velocity components, $\bar{U}$ and $\bar{V}$, respectively, were used to provide a streamline originating at the exit of the jet that is defined as the centerline trajectory. Experimental uncertainty in velocities ranged from approximately 3% to 5%, depending on test conditions, which translated to a maximum variation in 1.7% in the downstream trajectory of each centerline. Variations in density were not considered in this study for the reason given above.

2.2. Experimental Results

The resulting jet centerlines from the various flow regimes are shown in Figure 2. As we would expect, the higher the R_v value, the greater the effect of the cross wind in bending the jet. Note that when $R_v = 10.3$ with the active grid, the trajectory bends further downward than when $R_v = 10.5$ with the passive grid. This indicates that increased turbulence intensity translates to increased bending.

2.3. One-Dimensional Plume Model (Plumeria)

One-dimensional plume models are used as inversion tools to infer *MER* from plume height, or vice versa. This study makes use of the 1-D model, Plumeria (Mastin, 2014; Mastin et al., 2009). In a recent intercomparison study of plume models, Plumeria provided results similar to other models (Costa et al., 2016). Plumeria applies a control volume numerical method and requires source condition inputs (e.g., vent diameter, flow speed, and water content) and environmental inputs (e.g., vent elevation and weather data) to solve for plume axis and height. Plumeria accounts for both local weather and humidity effects but ignores particle fallout. The model outputs the centerline point position and plume height, integrating upward from the source until reaching an upper threshold where the plume has effectively stopped rising. Cross wind v_{wind} is decomposed into radial $v_\perp$ and axial $v_\parallel$ components (Figure 3). For this study, Plumeria was modified to use neutrally buoyant air as the jet fluid and to use step sizes appropriate for laboratory-scale experiments.

Figure 3. Volcanic plume control volume representation.

Plumeria solves for mass, momentum, and energy that allows calculation of changes in rate of mass flow M, momentum flow J, and energy flow E. The change in mass flow rate along the centerline s is given as follows:

$$\frac{dM}{ds} = 2\pi r \rho_{atm} \left[(\alpha(|u - v_\parallel|))^n + (\beta(|v_\perp|))^n \right]^{(1/n)} \quad (2)$$

Here, r is the radius of the control volume and ρ_{atm} is the atmospheric density. The two entrainment factors are superposed following the root-sum method of Devenish et al. (2010), which raises the entrainment terms individually using an exponent n, and their sum is raised by an exponent $1/n$. Unlike simple linear superpositions, this allows one-dimensional models to agree better with three-dimensional plume models in cases where the terms are of similar magnitude, such as the bending region (Mastin, 2014). For the iterations conducted here, $n = 1.5$, consistent with findings of optimal values of n from both Devenish et al. (2010) and Aubry et al. (2017).
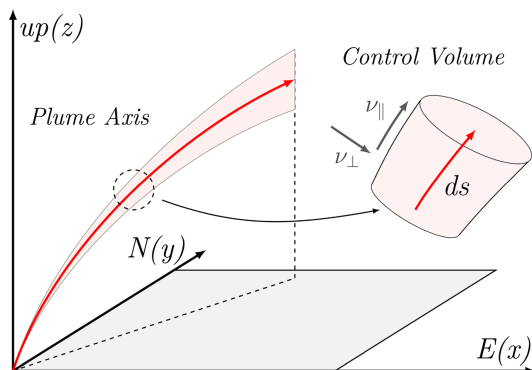
Of note, equation (2) assumes self-similar entrainment conditions for α, which occur after the momentum-driven region near the vent gives way to the convective region constituting the remainder of the plume. Within the initial (gas-thrust) region, the entrainment profile is developing toward a self-similar condition (Solovitz & Mastin, 2009) but is not yet self-similar. The entrainment coefficients are lower in the first few diameters near the vent. In addition, the entrainment scales with gas density, requiring rescaling of the mass flux by $\sqrt{\rho \rho_{atm}}$ (Thring, 1953). Thus, for the gas-thrust region, mass conservation is given as follows:

$$\frac{dM}{ds} = 2\pi r \sqrt{\rho \rho_{atm}} \left[(\alpha(|u - v_\parallel|))^n + (\beta(|v_\perp|))^n \right]^{(1/n)} \tag{3}$$

For the cases considered here, the developing region is a small portion of the trajectory, and the jet air density matches freestream air density. Hence, the behavior is only negligibly different in the gas-thrust region.

Plumeria assumes the jet/plume flow is inviscid; thus, in the momentum conservation equation the plume pressure is continuously equilibrated with ambient pressure. Therefore, changes in vertical momentum (J) result from plume buoyancy and changes in horizontal momentum result from the velocity, v_{wind}, of entrained air:

$$\frac{dJ_{x,y}}{ds} = \frac{dM}{ds} v_{wind_{x,y}} \tag{4}$$

$$\frac{dJ_z}{ds} = \pi r^2 (\rho_{atm} - \rho)g \tag{5}$$

Energy exchange is assumed to only be through advection across the air/plume interface (e.g., Mastin, 2007, Woods, 1988). Energy conservation is given as follows:

$$\frac{dE}{ds} = \frac{d}{ds} \left[M \left(\frac{u^2}{2} + gZ + h \right) \right] = (gZ + h_{atm}) \frac{dM}{ds} \tag{6}$$

where u is the centerline plume velocity, g is gravity, Z is height at the center of the control volume, and h and h_{atm} are local and atmospheric enthalpies, respectively.

At each position along the centerline, Plumeria uses local fluid and atmospheric conditions to explicitly evaluate the properties at the next downstream position. This process continues until the vertical jet velocity reaches approximately zero, which is the peak height H. When conditions at the exit and entrainment coefficients are known, the equations are closed and Plumeria predicts MER/H inversion values. For cases when the exit conditions are unknown, the model is run iteratively to determine the appropriate MER to match the observed H_{obs}.

3. Analysis

Plumeria model runs were performed using conditions identical to the wind tunnel experiments, systematically sampling over a range of entrainment coefficient values ($0.02 \leq \alpha \leq 0.17, 0.30 \leq \beta \leq 0.98$) along increments of 0.005 and 0.02, respectively. The values selected encompass the measured range for developing and fully developed conditions in the literature. In all, 1,085 iterations of Plumeria were generated for comparison with each experimental centerline generated during the wind tunnel measurements.

Statistical analysis was employed to compare the bending region of each Plumeria prediction to that of the experimental centerline. Regression curve fitting was used to minimize deviations between the model-predicted and experimental locations along the trajectory. The correlation coefficient for each α-β combination was calculated according to the formula:

$$R_{\alpha,\beta}^2 = 1 - \sum_i \frac{(y_{jet,i} - f_{Plumeria,i})^2}{(y_{jet,i} - \bar{y}_{jet})^2} \tag{7}$$

Here, $y_{jet,i}$ is the jet centerline elevation at a particular x distance downstream, $f_{Plumeria,i}$ is the corresponding Plumeria centerline value at that x location, and $\bar{y}_{jet}$ is the mean of all measured values (Figliola & Beasley, 1995).
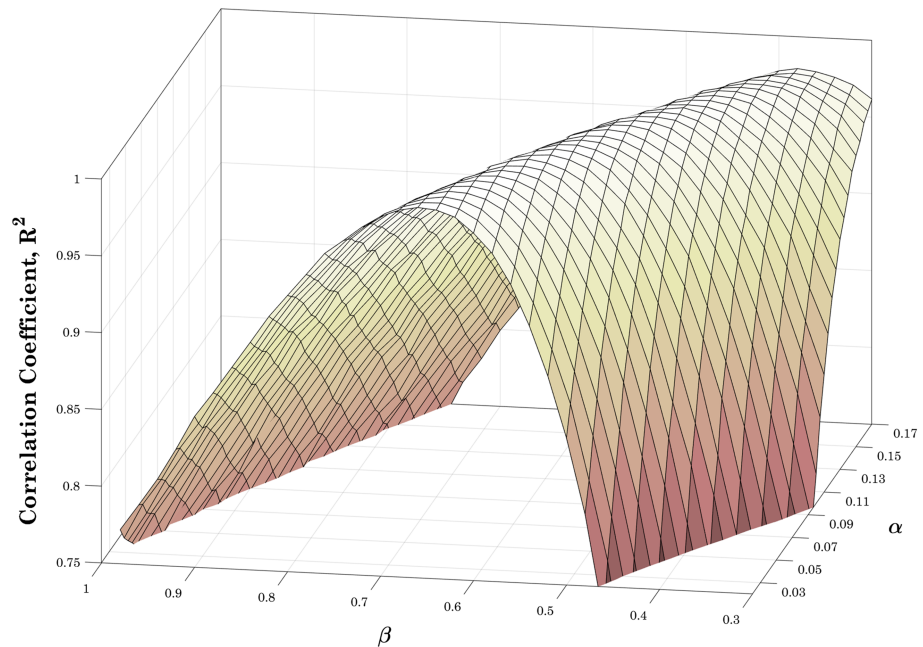
Figure 4. Response surface from centerline comparison. The x axis represents the various α inputs, the y axis represents β values, and the z axis shows the resulting R^2 value. (For ease of visibility, values below $R^2 = 0.75$ are not shown.)

The statistical analysis resulted in assignment of a correlation coefficient to each Plumeria output. A resulting response surface of the correlation coefficient is organized by entrainment coefficient configuration and is mapped to a grid (Figure 4). The uppermost region of the surface reflects the α-β combination that produced trajectory estimates most closely aligned with the experimental jet trajectory.

All of the response surfaces resulting from this analysis share the same overall shape and demonstrate several important trends about the optimal entrainment coefficients. First, rather than a single peak, there is a ridge of points that all have similar effectiveness in matching the experimental data. The linearity of the ridge indicates an approximately linear relationship between α and β values that produce best fit combinations, where increasing α sees a decreasing β. This may explain why different one-dimensional models have performed similarly with differing entrainment coefficients (Costa et al., 2016). Additionally, the response surface demonstrates clear disparity between the impact of α and β on model accuracy. For the case shown, we can see that model accuracy is more sensitive to relative changes in β than to those of α, as the correlation coefficient falls off much more rapidly with variations in β (Figure 4).

The α-β relationship was further explored by isolating the best fit α-β pairs for each experimental case, considering all velocity ratios and turbulence conditions. Based on the response surface data, the best fit β was interpolated from each α value. The resulting pairs were then plotted according to their corresponding experimental case, as shown in Figure 5. For each value of R_v, the best fit α-β relationship is approximately linear. The trend lines show that an increase in α corresponds to a decrease in β. The slopes of these lines are similar for most cases, though the magnitude is higher with greater R_v, corresponding to the strongest plumes.

Mean β and standard deviation were calculated at each α. Convergence occurs at $\alpha = 0.06$ with markedly different β depending on turbulence regime. In the active grid cases, best fit lines converged at $\beta = 0.52$. Passive grid cases converged at $\beta = 0.46$. When averaged, convergence is at $\alpha = 0.06, \beta = 0.49$. However, since the turbulence kinetic energy in Active grid regime (TI 10–15%) is higher than atmospheric levels above the boundary layer (i.e., most of the plume), this upper value is less pertinent. Thus, we can consider $\beta = 0.46$ as the optimal value for most eruptive cases. At this α, standard deviation is <1%. The wide range of R_v and $\alpha - \beta$ configurations show the β/α ratio is not a constant as suggested in previous studies (e.g., Aubry et al., 2017; Carazzo et al., 2014). However, Figure 5 shows that the best fit β coefficient value converges at $\alpha = 0.06$, consistent with previous laboratory studies (e.g., Fischer et al., 1979).
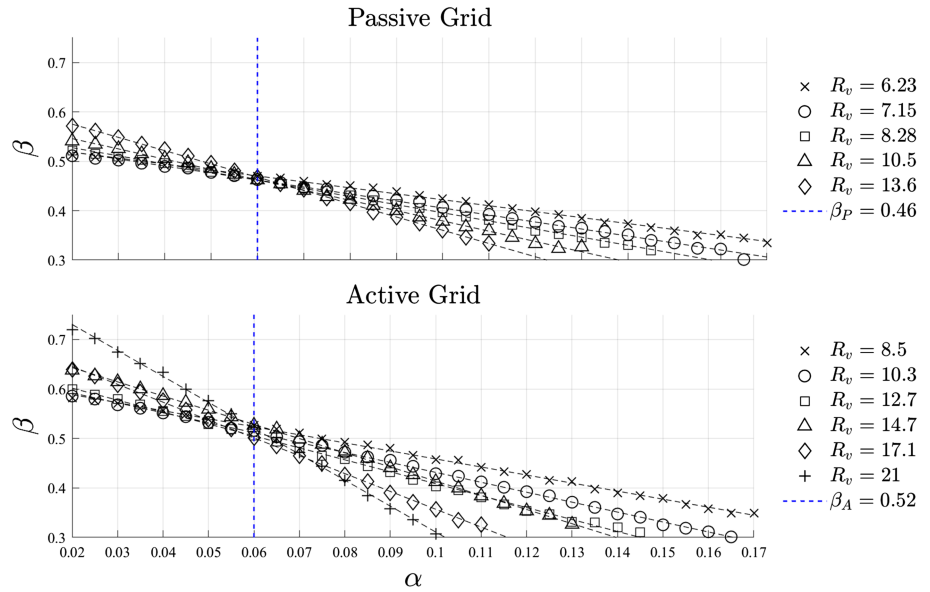
Figure 5. Best fit entrainment coefficients for various R_v and turbulence conditions. Iterations that incorporated experimental uncertainty described in section 2.2 did not significantly affect best fit coefficients. For each R_v, the average best fit coefficient $\bar{R}^2_{best}$ value along $0.02 \leq \alpha \leq 0.17$ was at least 0.94 with a standard deviation of less than 3%.

4. Application to Volcanic Eruptions

Historical eruption data are often used as benchmark when evaluating modifications made to 1-D plume models. New configurations are set in the model, and its output is compared to previous results to see if it better approximates eruption data. Here, several eruptions with independently estimated MER_{obs} and H_{obs} values were chosen, encompassing a spectrum of wind effects and MER_{obs}. Comparisons are also made with the correlation reported by Mastin et al. (2009), which relates MER_{obs} (in kg/s) to H_{obs} (in km) and is based on theoretical relationships from averaged eruption data (Mastin et al., 2009). The given relationship is:

$$MER_{0-D} = 140H_{obs}^{4.15} \qquad (8)$$

The eruptions chosen are shown in Table 2. These span a range of eruption rates and weather conditions. MER is obtained by dividing erupted mass by duration D. MER_{obs} uncertainty was calculated by propagating uncertainties published in Aubry et al. (2017) (supplemental). In cases where duration differs slightly from Aubry et al. (2017) (supplemental), MER_{obs} uncertainty is calculated using relative M and D uncertainties. In the case of Eyjafjallajökull (2010), the values used represent a short duration on 17 April 2010 as reported by Mastin (2014) and Arason et al. (2011). In the case of the 22 and 23 April 2015 eruptions of Calbuco, the two distinct events are considered individually.

The analysis had three parts. First, the plume height was evaluated using the previously determined optimal α-β combination ($\alpha = 0.06$, $\beta = 0.46$), testing the accuracy of the modified entrainment coefficients. In general, there is not a perfect match due to measured uncertainties. Second, β was varied from 0 to unity to establish which, if any, value coincided with the observed H_{obs}; α was held constant at 0.06, since β has a stronger influence on the response, as seen in Figures 4 and 5. This helps identify if there is any correlation between field conditions and preferred β values. Third, MER was incremented at the optimal α-β configuration to find which value resulted in an accurate H_{obs} prediction by the model. This effectively performs the inversion process required for ash transport forecasting.

The source parameter assumptions used in Plumeria follow previous analyses (Costa et al., 2016; Mastin, 2014). Weather data were taken from the National Centers for Environmental Prediction/National Center for Atmospheric Research Reanalysis 1 model (Kalnay et al., 1996). Condensation of water vapor and its potential effect on the plume buoyancy flux are incorporated in the model. Typical property values were selected, with a magma specific heat of 1,000 J/(kg * K), temperature of 930 °C, and density of 2,500 kg/m³. For iterations where MER was matched to Table 2, the centerline velocity (u) was set to 150 m/s, and the

Table 2
Historical Eruptions Chosen to Evaluate Plumeria Modifications

Eruption	Date	Time (UTC)	$D(D_\pm)$ (hr)	$H_{obs}(H_{obs\pm})$ (km a.v.l.)	R_v^i	$MER_{obs}(MER_{obs\pm})$ (kg/s)
Cabulco(1)[a,b]	04/22/2015	21:04	1.50 (0.25)	15.0 (2.5)	13.5	6.00E+6 (3.53E+6)
Cabulco(2)[a,b]	04/23/2015	3:54	6.00 (0.25)	17.1 (3.0)	13.2	8.05E+6 (2.42E+6)
Cordon Caulle(1)[b]	06/04/2011	18:30	27 (3)	10.5 (2)	7.57	4.32E+6 (1.41E+6)
Cordon Caulle(2)[b]	06/07/2011	5:00	7.5 (4.5)	9.5 (3)	4.72	4.81E+6 (4.37E+6)
Cordon Caulle(3)[b]	06/07/2011	11:00	7.5 (4.5)	6 (3)	5.24	1.04E+6 (8.81E+5)
Etna[b,c]	11/24/2006	2:30	10 (1)	1.65 (0.35)	15.2	5.00E+3 (2.17E+3)
Eyjafjallajökull[d,e]	04/17/2010	20:03	0.07 (0.01)	3.5 (0.25)	11	2.45E+5 (8.78E+4)
Kelud[b,f,g,h]	02/13/2014	15:50	2.75 (0.75)	19.5 (3)	12.9	4.00E+7 (2.40E+7)
Mount St Helens[b,c]	05/25/1980	9:30	0.5 (0.38)	10.2 (1.5)	19.4	2.00E+7 (1.30E+7)
Pinatubo[b,c]	06/12/1991	0:51	0.63 (0.3)	17.5 (4)	43.5	6.00E+6 (5.00E+6)
Reventador[b,c]	11/03/2002	15:10	22 (12.57)	17 (6.6)	25.3	1.00E+7 (7.94E+6)
Ruapehu[b,c]	06/17/1996	0:00	6.50 (1.5)	5.7 (2)	6.56	5.00E+5 (9.83E+4)
Shinmoedake(1)[b]	01/26/2011	7:10	3.25 (0.75)	5.8 (1.3)	5.06	9.74E+5 (4.73E+5)
Shinmoedake(2)[b]	01/26/2011	12:45	4.5 (1)	3.4 (1.3)	8.34	2.19E+5 (1.04E+5)
Shinmoedake(3)[b]	01/26/2011	17:20	2.75 (0.25)	6.1 (1)	5.45	1.52E+6 (5.22E+5)
Shinmoedake(4)[b]	01/27/2011	7:20	2.00 (0.30)	6.0 (1)	6.18	1.18E+6 (4.69E+5)
Spurr(1)[b,c]	08/18/1992	1:43	3.6 (0.33)	10.5 (3)	8.32	3.00E+6 (1.43E+6)
Spurr(2)[b,c]	09/17/1992	9:00	3.5 (0.33)	10.7 (2)	6.14	3.00E+6 (1.47E+6)
Tungurahua(1)[b]	08/17/2006	2:13	2.5 (1.5)	14.5 (3)	29.2	2.77E+6 (2.35E+6)
Tungurahua(2)[b]	07/14/2013	11:47	1.25 (0.25)	6.7 (1.7)	22.4	1.49E+5 (4.09E+4)

Note. Variables shown are duration D, observed plume height H_{obs} above vent level (a.v.l.), jet-to-wind ratio R_v, and mass eruption rate MER_{obs}. Uncertainty associated with D, H_{obs}, and MER_{obs} ($\pm$) is shown in parentheses. Dates are formatted as MM/DD/YYYY.
[a]Van Eaton et al. (2016). [b]Aubry et al. (2017) (supplemental). [c]Mastin et al. (2009). [d]Mastin (2014). [e]Arason et al. (2011). [f]Kristiansen et al. (2015). [j]Maeno et al. (2017). [h]Vernier et al. (2016). [i]R_v calculated according to formula (1) by averaging local wind velocities during the eruption (Kalnay et al., 1996), and assuming a vent exit velocity of 150 m/s. Based on vent exit velocity estimates by Woods and Bower (1995), R_v uncertainty ($\pm R_v$) is a factor of ~1.

vent diameter was adjusted. This value was selected because it did not lead to column collapse in previous analyses (Mastin, 2014). Based on vent exit velocity estimates by Woods and Bower (1995), R_v uncertainty ($\pm R_v$) is a factor of ~1.

The first goal of the analysis was to establish whether α and β refinement improved the accuracy of plume height estimates, H_{Old}, produced by Plumeria. Plumeria defines plume height as the height of the centerline plus the radius at the top of the plume (Mastin, 2007, 2014). Iterations were conducted for each eruption using both the baseline ($\alpha = 0.09$; $\beta = 0.50$) and the revised entrainment coefficient configuration ($\alpha = 0.06$; $\beta = 0.46$), resulting in H_{New}. These values were selected based on the results of the analysis described in section 2 because the inflow turbulence intensity in the passive grid cases better approximates a wider range of real-world conditions. Aircraft-based measurements report midatmospheric turbulence intensities well below 10% (e.g., Riedel & Sitzmann, 1998). These predictions are compared to both the observed plume height, H_{obs}, and the estimate from the simple correlation in equation (8), H_{0-D}. The results of the analysis are shown in Figure 6. Each of the eruptions from Table 2 is presented, with all four values for plume height depicted. The data are presented in order of observed plume height.

In all cases, the revised α-β combination resulted in larger predicted H, with the difference approximately scaling with MER_{obs}. By reducing the entrainment coefficient values, the predicted plume trajectory bends more slowly, permitting higher peak heights. For example, the difference between H_{New} and H_{Old} was 250 m for Eyjafjallajökull and 1,160 m for Kelud. In 18 of the 20 eruptions, the modified plume model also produces better predictions of the observed height, although in several cases the change was not significant. In most
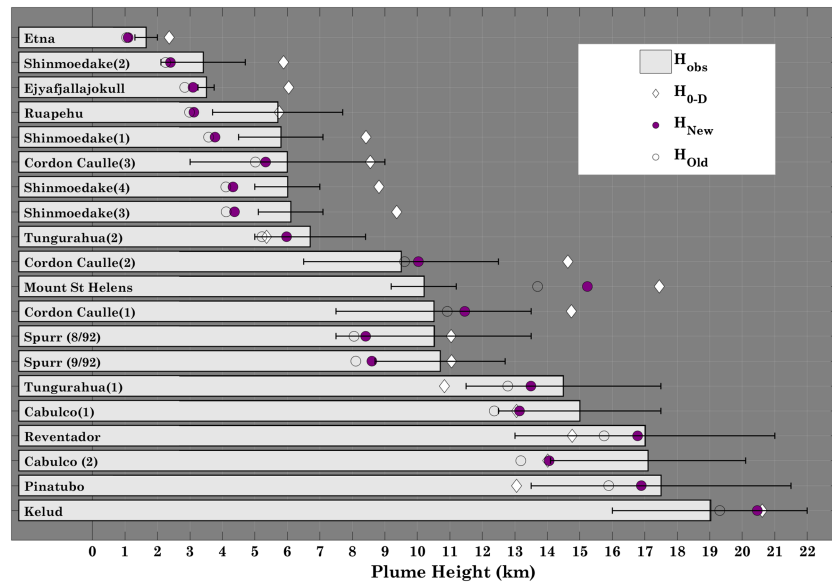
Figure 6. Comparisons of plume height predictions from correlations (H_{0-D}) and plume models before and after α and β revision (H_{Old} and H_{New}, respectively) with observed plume height (H_{obs}). Error bars represent uncertainty in H_{obs} ($H_{obs\pm}$).

cases, the simulated height was within 3 km of the observed height, with agreement to within approximately 1 km for stronger eruptions like Reventador, Pinatubo, and Kelud.

Predictions for stronger eruptions with higher R_v generally showed better agreement than weaker plumes. For eruptions with lower plume heights ($H_{obs} < 7$ km), Plumeria underpredicted plume height using both the original and revised entrainment coefficients, while equation (8) usually overpredicted it, as noted previously (Mastin, 2014). Plumes with $H_{obs} < 7$ km represent cases where cross-wind effects on the plume were greatest, with R_v between 3 and 11. Within this range, the differences between H_{Old} and H_{New} are smallest, resulting in only modest improvement in agreement with observations. More importantly, lower plume heights correspond to cases where MER estimation has its highest uncertainty (Woodhouse et al., 2015). Mount St. Helens is a unique case, which has shown significant discrepancies with previous models. Carey et al. (1990) attributed the disparity between H_{obs} and MER_{obs} to underestimation of pyroclastic flow generations during the first hours of the eruption, which added to the mass. Degruyter and Bonadonna (2012) argue that the unusually low plume height can be attributed primarily to the wind. Recent studies suggest eruption style impacts plume generation (e.g., Gouhier et al., 2019), which may play a role in the seemingly anomalous H_{obs} of this eruption. Hence, while total erupted volume is well-constrained, H_{obs} - MER discrepancies persist, and deviations are not unexpected with this eruption.

Since there were still some discrepancies between observed and simulated plume heights, the second stage of the analysis considered what value of β would be needed to match H_{obs}. Figure 7 shows the required β value versus the cross-wind velocity ratio, R_v, for each of these cases. Not shown are Mount St. Helens, Calbuco(2), Pinatubo, and Tungurahua(2), where agreement with H_{obs} was not reached for $0 \leq \beta \leq 1.0$. The former case is unique, with discrepancies in each of the predictive tools, while the latter cases agreed to within 3 km. Plume height uncertainty, $\pm H_{obs}$, was not considered in this portion of the analysis. We note that the sweep of H_{New} and H_{Old} for $0.03 \leq \beta \leq 0.98$ ranged from ~1.5 km to ~3 km, roughly on the order of $\pm H_{obs}$ for the four cases that did not find agreement.

There is a general trend here, showing that β must be reduced significantly to match the observed height for weaker plumes. For the smallest R_v, at Cordon Caulle(2), β must be near 0.33, much as shown by Suzuki and Koyaguchi (2015). In fact, all of the weak plumes required a reduced β value. For the strong plume at Kelud, the value is closer to 0.46, which is more comparable to the optimal case. Intriguingly, every other eruption required $\beta < 0.46$ to match H_{obs}. Calbuco(1) actually required a much lower β than Kelud at a comparable R_v, though it still agreed to within 2 km at $\beta = 0.46$.
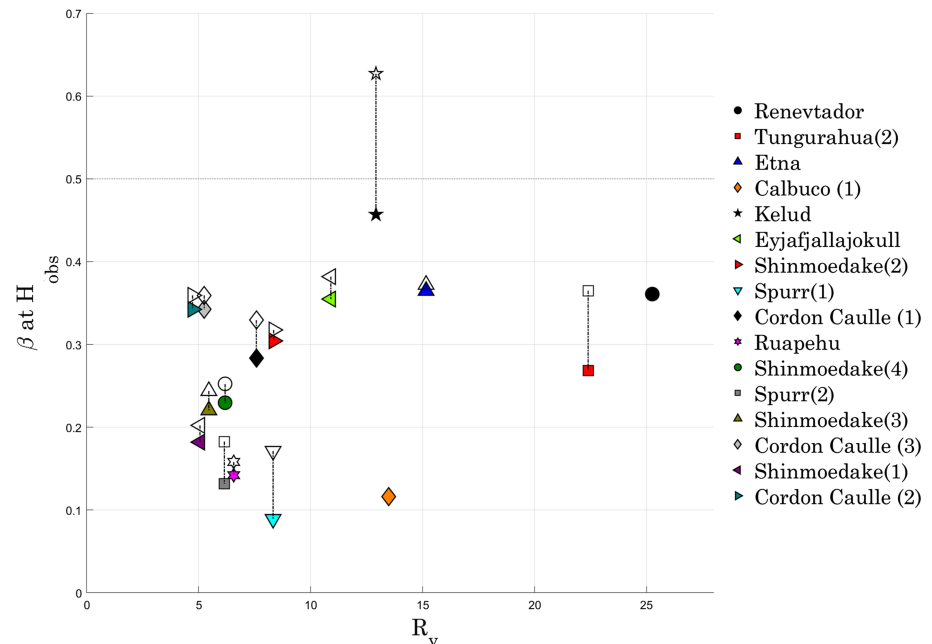
Figure 7. Cross-flow entrainment coefficient, β, required to produce the observed plume height, H_{obs}, at various cross-flow velocity ratios, R_v, using the plume model with optimal α and β (filled, $\alpha = 0.06$) and compared with previous α-β (open, $\alpha = 0.09$). For four cases (Calbuco(2), Mount St. Helens, Tungurahua(2), and Pinatubo), Plumeria did not predict H_{obs} at $0 \leq \beta \leq 1.0$. For Reventador and Cabulco(1), agreement with H_{obs} was not reached for $\alpha = 0.09$ at $0 \leq \beta \leq 1.0$.

The lower β that best fits with H_{obs} is different from what is expected in Figure 5. The discrepancy could be related to at least two factors: (1) The large uncertainty in both plume height and eruption rate of the real eruptions and (2) disparity in how the maximum plume height might be defined in the model. This application of Plumeria uses the height of the centerline, consistent, for example, with plume heights used in the model intercomparison of Costa et al. (2016), rather than the centerline plus radius, as given, for example, in Mastin (2014). Models that define plume height differently would require different α-β configurations to match H predictions for a given eruption with a known MER_{obs}.

The third stage of the analysis was based on the typical field use of a 1-D model, where the observed height is inverted to determine the MER. Plumeria iterations were performed to match MER_{obs} to H_{obs} for each eruption, considering both the baseline and optimal α-β combinations. Figure 8 shows the predicted MER_{Old} and MER_{New} for each eruption, reflecting the α-β configuration, along with the value from the empirical correlation, MER_{0-D}. As before, the optimized α-β combination resulted in improved model accuracy in 18 of the 20 cases. All agree with the observed MER_{obs} to within a factor of 10, with most to within a factor of 3. Several eruptions are very closely matched, notably Pinatubo, Reventador, and Kelud.

Validation of improvements to 1-D plume models is made challenging by uncertainties in eruption field data. Variations in estimations of historical data culminate in uncertainty bands that vary greatly, especially those pertaining to data acquisition and processing (Biass & Bonadonna, 2011; Bonadonna et al., 2012, 2015; Fierstein & Nathenson, 1992; Macedonio et al., 2016; Mastin et al., 2009). Particularly challenging are weaker plumes, where equation (8) predicts a rapid increase in MER with increasing plume height. This limitation is shown in Figure 8, where discrepancies with field data for weaker eruptions increase as MER decreases.

Three of the weaker plumes in Table 2 had specific challenges for field analysis. The August 1992 Mount Spurr eruption had fallout over the Gulf of Alaska, while the September 1992 eruption had fallout over both Cook Inlet and the Wrangell mountain range (Rose et al., 1995). These locations were difficult or impossible to access directly, increasing the uncertainty in the MER_{obs}. The 1996 eruption at Ruapehu, while well characterized, showed significant unsteadiness, with plume heights differing by several kilometers over the course of the eruption (Bonadonna & Houghton, 2005). Because source parameter uncertainty in real-world
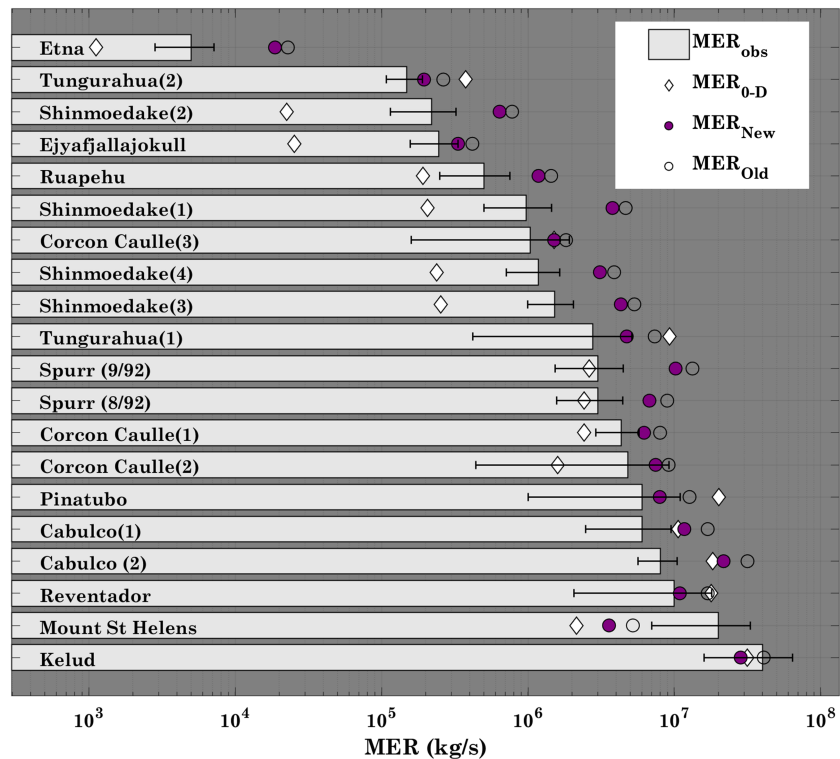
Figure 8. Results of the MER inversion iterations to gauge model improvement after α-β refinement.

eruptions outweighs that of the experimental data, any validation will be limited by the quality of the input field observations.

However, there is an alternate method of validation that better correlates to the PIV experimental data. Rather than basing the comparison on simply the final observed height, observed plume trajectories can be used, much as are considered in the laboratory. Webcam footage from the April 2010 eruption of Eyjafjallajökull (Arason et al., 2011) is used to determine the centerline path and scaled centerlines from Plumeria are plotted directly onto time-averaged images. This provides a more direct comparison of the effectiveness of α-β optimization.

Volcano observatories in Iceland continuously monitor all volcanic activity, relocating sensors whenever an eruption begins. Consequently, a portion of the Eyjafjallajökull eruption was recorded via webcam from the village of Hvolsvöllur, located 34 km northeast of the volcano. Figure 9 shows a representative image taken 10 May 2010, with vertical scaling superimposed.

The Hvolsvöllur webcam footage consists of images captured at 5-s intervals by a fixed camera with a viewing window extending to about 5.2 km ASL, or about 3.5 km above the vent (Björnsson et al., 2013). Resolved vertical image resolution is about 15 pixels per 100 m. Although the camera was monitoring the eruption for the entire duration of 39 days, visibility impairment due to weather conditions prevented a clear view of the vent for all but a few days. The images used for this analysis were taken between 20:03 and 20:07 UTC on 17 April 2010 (Arason et al., 2011).

The webcam footage has been the subject of several studies (Arason et al., 2011; Björnsson et al., 2013; Petersen et al., 2012), so eruption characteristics for this time period are well established. Plume height was 5.1 km ASL, averaged from data downloaded from supplemental materials in Arason et al. (2011). *MER* estimates were based on Mastin (2014), using 10E+5.1 kg/s, which corresponds well with the earlier studies. Weather data were taken from the National Centers for Environmental Prediction/National Center for Atmospheric Research Reanalysis 1 model (Kalnay et al., 1996). The plume trajectory was postprocessed to account for geometric issues, as the plume was not perpendicular to the camera. Björnsson et al. (2013) estimated that the winds deviated from the plane by 17–21°, with average velocities of 14 m/s. Thus, the plume
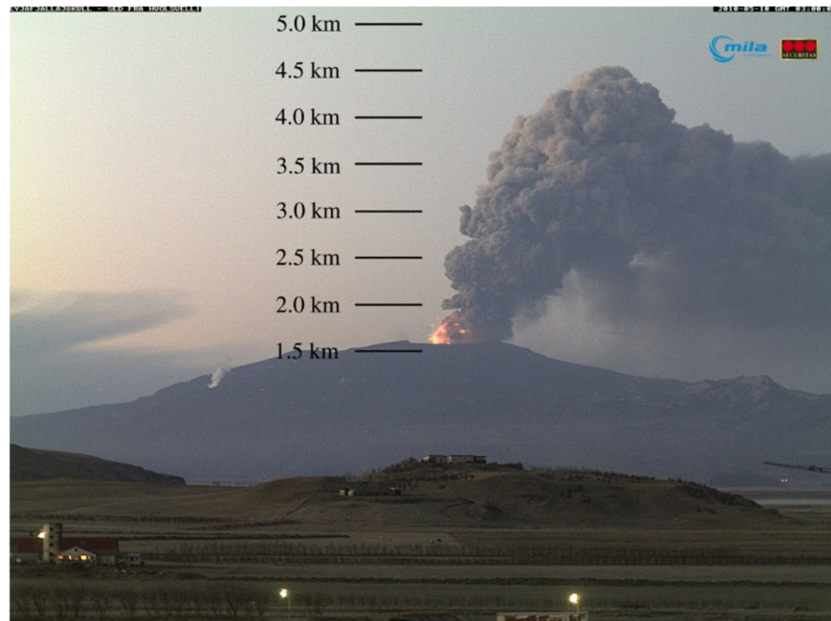
Figure 9. Image of Eyjafjallajökull eruption from Hvolsvöllur webcam, shown with reference altitude (Arason et al., 2011). *Image used with permission.*

was assumed to be rotated away from the viewing plane by 19°, which skews the apparent plume height by approximately 6%.

The webcam images were compared to estimated plume trajectories by superimposing output centerlines from Plumeria onto the footage. As before, two plume models were considered: one with the baseline α-β combination ($\alpha = 0.09$, $\beta = 0.50$) and the other with the experimentally derived α-β combination ($\alpha = 0.06$, $\beta = 0.46$). The model output was rescaled to reflect the orientation of the image, assuming a constant trajectory out of plane. The camera image files were time-averaged to provide a visual sense of the plume's domain. Figure 10 shows the resulting image, with the centerlines applied.
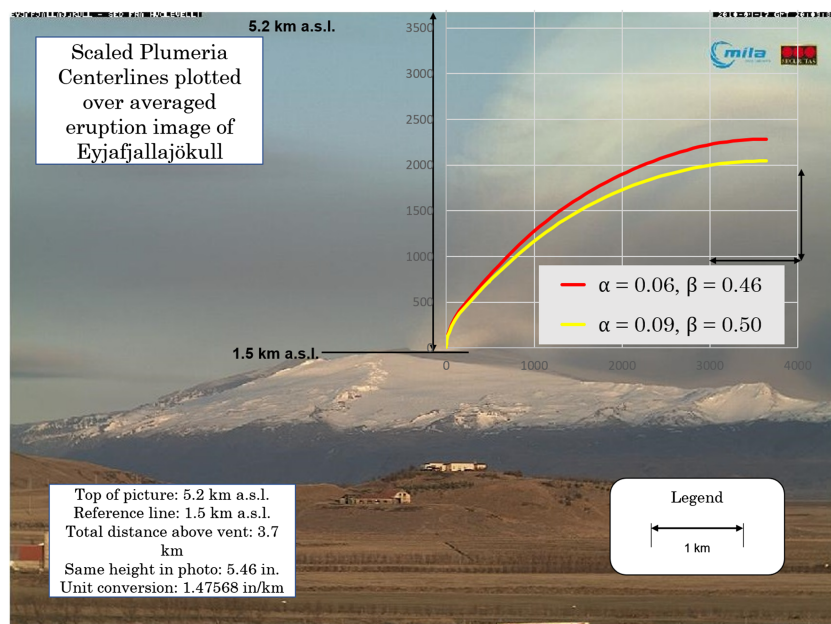

Figure 10. Plumeria centerline comparison for Eyjafjallajökull.

Based on the comparison, several trends are apparent. First, both estimated centerlines approximately trace the centerline of the plume, passing through the middle of the cloud. This indicates that either α-β combination can predict the basic trajectory in this bending region. Second, the centerlines are similar due to the small α-β adjustment, but the adjustment does lead to a slightly higher plume path, differing by more than 10% at the end of the simulation. Third, the plume occupies a wide range on either side of the predicted trajectory. This suggests that the entrainment coefficients could be modified significantly while still remaining within the visible plume, further justifying why a range of β values have been applied previously.

5. Conclusions

The accuracy of entrainment coefficients in the one-dimensional plume model Plumeria was explored through experiments, iterative data analysis, and real-world verification. Velocity field measurements in a wind tunnel showed that atmospheric turbulence increases the bending effect, indicative of increased entrainment. Regression analysis of the plume model iterations was used to generate response surfaces, which showed the impact of each entrainment coefficient on model predictions.

The vertical and cross-flow entrainment coefficients, α and β, have an approximately linear relationship with each other, even when cross-flow turbulence intensities were increased. This interdependence helps to explain variations between parameter selections found in previous studies. At different cross-flow velocity ratios, there is a convergence of these optimal curves for a particular combination of α and β. Based on comparison of the α-β lines for all experimental cases, the optimal entrainment coefficients were $\alpha = 0.06$ and $\beta = 0.46$.

While curve matching with experimental cases yielded convergence on a best fit α-β configuration, the results had mixed success in comparisons of plume height with historical eruption data. The optimized α-β relationship improved estimates in most cases, but they generally did not alter plume height predictions from the model enough to match observed plume heights. Decreasing values of β were needed to match observations, especially in weak plumes, suggesting a strong dependence on cross wind. MER predictions agreed with field data to within a factor of 3 in most cases. Even so, with weak plumes, the variations in field data dwarfed the experimental uncertainties, making close comparisons with historical eruption data challenging. However, predicted trajectories agreed well with webcam images of the 2010 Eyjafjallajökull eruption.

References

Agrawal, A., & Prasad, A. K. (2003). Integral solution for the mean flow profiles of turbulent jets, plumes, and wakes. *Journal of Fluids Engineering*, *125*(5), 813–822. https://doi.org/10.1115/1.1603303

Arason, P., Petersen, G. N., & Bjornsson, H. (2011). Observations of the altitude of the volcanic plume during the eruption of Eyjafjallajökull, April-May 2010. *Earth System Science Data*, *3*(1), 9–17. https://doi.org/10.5194/essd-3-9-2011

Aubry, T. J., Jellinek, A. M., Carazzo, G., Gallo, R., Hatcher, K., & Dunning, J. (2017). A new analytical scaling for turbulent wind-bent plumes: Comparison of scaling laws with analog experiments and a new database of eruptive conditions for predicting the height of volcanic plumes. *Journal of Volcanology and Geothermal Research*, *343*, 233–251. https://doi.org/10.1016/j.jvolgeores.2017.07.006

Baines, W. D. (1983). A technique for the direct measurement of volume flux of a plume. *Journal of Fluid Mechanics*, *132*, 247–256. https://doi.org/10.1017/S0022112083001585

Biass, S., & Bonadonna, C. (2011). A quantitative uncertainty assessment of eruptive parameters derived from tephra deposits: The example of two large eruptions of Cotopaxi volcano, Ecuador. *Bulletin of Volcanology*, *73*(1), 73–90. https://doi.org/10.1007/s00445-010-0404-5

Björnsson, H., Magnusson, S., Arason, P., & Petersen, G. N. (2013). Velocities in the plume of the 2010 Eyjafjallajökull eruption. *Journal of Geophysical Research: Atmospheres*, *118*, 11,698–11,711. https://doi.org/10.1002/jgrd.50876

Bonadonna, C., Biass, S., & Costa, Antonio (2015). Physical characterization of explosive volcanic eruptions based on tephra deposits: Propagation of uncertainties and sensitivity analysis. *Journal of Volcanology and Geothermal Research*, *296*, 80–100. https://doi.org/10.1016/j.jvolgeores.2015.03.009

Bonadonna, C., Folch, A., Loughlin, S., & Puempel, H. (2012). Future developments in modelling and monitoring of volcanic ash clouds: Outcomes from the first IAVCEI-WMO workshop on ash dispersal forecast and civil aviation. *Bulletin of Volcanology*, *74*(1), 1–10. https://doi.org/10.1007/s00445-011-0508-6

Bonadonna, C., & Houghton, B. F. (2005). Total grain-size distribution and volume of tephra-fall deposits. *Bulletin of Volcanology*, *67*(5), 441–456. https://doi.org/10.1007/s00445-004-0386-2

Briggs, G. A. (1965). A plume rise model compared with observations. *Journal of the Air Pollution Control Association*, *15*(9), 433–438. https://doi.org/10.1080/00022470.1965.10468404

Briggs, G. A. (1984). Plume rise and buoyancy effects. *Atmospheric science and power production*, *850*, 327–366.

Bursik, M. (2001). Effect of wind on the rise height of volcanic plumes. *Geophysical Research Letters*, *28*(18), 3621–3624. https://doi.org/10.1029/2001GL013393

Carazzo, G., Girault, F., Aubry, T., Bouquerel, H., & Kaminski, E. (2014). Laboratory experiments of forced plumes in a density-stratified crossflow and implications for volcanic plumes. *Geophysical Research Letters*, *41*, 8759–8766. https://doi.org/10.1002/2014GL061887

Carey, S., Sigurdsson, H., Gardner, J. E., & Criswell, W. (1990). Variations in column height and magma discharge during the May 18, 1980 eruption of Mount St. Helens. *Journal of Volcanology and Geothermal Research*, *43*(1), 99–112. https://doi.org/10.1016/0377-0273(90)90047-J

Costa, A., Suzuki, Y. J., Cerminara, M., Devenish, B. J., Ongaro, T. Esposti, Herzog, M., et al. (2016). Results of the eruptive column model inter-comparison study. *Journal of Volcanology and Geothermal Research*, *326*, 2–25. https://doi.org/10.1016/j.jvolgeores.2016.01.017

Degruyter, W., & Bonadonna, C. (2012). Improving on mass flow rate estimates of volcanic eruptions. *Geophysical Research Letters*, *39*, L16308. https://doi.org/10.1016/j.epsl.2013.06.041

Devenish, B., Rooney, G., & Thomson, D. (2010). Large-eddy simulation of a buoyant plume in uniform and stably stratified environments. *Journal of Fluid Mechanics*, *652*, 75–103. https://doi.org/10.1017/S0022112010000017

Falcone, A. M., & Cataldo, J. C. (2003). Entrainment velocity in an axisymmetric turbulent jet. *Journal of fluids engineering*, *125*(4), 620–627. https://doi.org/10.1115/1.1595674

Fierstein, J., & Nathenson, M. (1992). Another look at the calculation of fallout tephra volumes. *Bulletin of Volcanology*, *54*(2), 156–167. https://doi.org/10.1007/BF00278005

Figliola, R. S., & Beasley, D. E. (1995). *Theory and design for mechanical measurements* (2nd ed.). Hoboken, NJ: IOP Publishing.

Fischer, H. B., List, E., Koh, R., Imberger, J., & Brooks, N. (1979). *Mixing in inland and coastal waters*. New York: Academic Press.

Freedland, G. (2016). Investigation of jet dynamics in cross-flow: Quantifying volcanic plume behavior (Ph.D. Thesis).

Gouhier, M., Eychenne, J., Azzaoui, N., Guillin, A., Deslandes, M., Poret, M., et al. (2019). Low efficiency of large volcanic eruptions in transporting very fine ash into the atmosphere. *Scientific reports*, *9*(1), 1449. https://doi.org/10.1038/s41598-019-38595-7

Hewett, T., Fay, J., & Hoult, D. (1971). Laboratory experiments of smokestack plumes in a stable atmosphere. *Atmospheric Environment (1967)*, *5*(9), 767IN3773–772789. https://doi.org/10.1016/0004-6981(71)90028-X

Hoult, D. P., Fay, J. A., & Forney, L. J. (1969). A theory of plume rise compared with field observations. *Journal of the Air Pollution Control Association*, *19*(8), 585–590. https://doi.org/10.1080/00022470.1969.10466526

Huq, P., & Stewart, E. (1996). A laboratory study of buoyant plumes in laminar and turbulent crossflows. *Atmospheric Environment*, *30*(7), 1125–1135. https://doi.org/10.1016/1352-2310(95)00335-5

Hussein, H. J., Capp, S. P., & George, W. K. (1994). Velocity measurements in a high-Reynolds-number, momentum-conserving, axisymmetric, turbulent jet. *Journal of Fluid Mechanics*, *258*, 31–75. https://doi.org/10.1017/S002211209400323X

Kalnay, E., Kanamitsu, M., Kistler, R., Collins, W., Deaven, D., Gandin, L., et al. (1996). The NCEP/NCAR 40-year reanalysis project. *Bulletin of the American meteorological Society*, *77*(3), 437–472. (formerly) https://www.esrl.noaa.gov/psd/

Kaminski, E., Tait, S., & Carazzo, G. (2005). Turbulent entrainment in jets with arbitrary buoyancy. *Journal of Fluid Mechanics*, *526*, 361–376. https://doi.org/10.1017/S0022112004003209

Karagozian, A. R. (2014). The jet in crossflow. *Physics of Fluids*, *26*(10), 1–47. https://doi.org/10.1063/1.4895900

Kristiansen, N. I., Prata, A. J., Stohl, A., & Carn, S. A. (2015). Stratospheric volcanic ash emissions from the 13 February 2014 Kelut eruption. *Geophysical Research Letters*, *42*, 588–596. https://doi.org/10.1002/2014GL062307

Macedonio, G., Costa, A., & Folch, A. (2016). Uncertainties in volcanic plume modeling: A parametric study using FPLUME. *Journal of Volcanology and Geothermal Research*, *326*, 92–102. https://doi.org/10.1016/j.jvolgeores.2009.01.008

Maeno, F., Nakada, S., Yoshimoto, M., Shimano, T., Hokanishi, N., Zaennudin, A., & Iguchi, M. (2017). A sequence of a plinian eruption preceded by dome destruction at Kelud volcano, Indonesia, on February 13, 2014, re593 vealed from tephra fallout and pyroclastic density current deposits. *Journal of Volcanology and Geothermal Research*. https://doi.org/10.1016/j.jvolgeores.2017.03.002

Mastin, L. G. (2007). A user-friendly one-dimensional model for wet volcanic plumes. *Geochemistry, Geophysics, Geosystems*, *8*, Q03014. https://doi.org/10.1029/2006GC001455

Mastin, L. G. (2014). Testing the accuracy of a 1-D volcanic plume model in estimating mass eruption rate. *Journal of Geophysical Research: Atmospheres*, *119*, 2474–2495. https://doi.org/10.1002/2013JD020604

Mastin, L. G., Guffanti, M., Servranckx, R., Webley, P., Barsotti, S., Dean, K., et al. (2009). A multidisciplinary effort to assign realistic source parameters to models of volcanic ash-cloud transport and dispersion during eruptions. *Journal of Volcanology and Geothermal Research*, *186*(1-2), 10–21. https://doi.org/10.1016/j.jvolgeores.2009.01.008

Morton, B. R., Taylor, G., & Turner, J. S. (1956). Turbulent gravitational convection from maintained and instantaneous sources. In *Proceedings of the royal society of London a: Mathematical, physical and engineering sciences*, *234*, The Royal Society. (pp. 1–23). https://doi.org/10.1098/rspa.1956.0011

Petersen, G. N., Bjornsson, H., & Arason, P. (2012). The impact of the atmosphere on the Eyjafjallajökull 2010 eruption plume. *Journal of Geophysical Research*, *117*, D00U07. https://doi.org/10.1029/2011JD016762

Pope, S. B. (2000). *Turbulent flows*, pp. 771. Cambridge, UK: Cambridge University Press.

Ricou, F. P., & Spalding, D. B. (1961). Measurements of entrainment by axisymmetrical turbulent jets. *Journal of Fluid Mechanics*, *11*(1), 21–32. https://doi.org/10.1017/S0022112061000834

Riedel, H., & Sitzmann, M. (1998). In-flight investigations of atmospheric turbulence. *Aerospace Science and technology*, *2*(5), 301–319.

Rose, W. I., Kostinski, A. B., & Kelley, L. (1995). Real-time C-band radar observations of 1992 eruption clouds from Crater Peak, Mount Spurr volcano, Alaska. *US Geological Survey Bulletin*, *2139*, 19–26.

Solovitz, S. A., & Mastin, L. G. (2009). Experimental study of near-field air entrainment by subsonic volcanic jets. *Journal of Geophysical Research*, *114*, B10203. https://doi.org/10.1029/2009JB006298

Su, L. K., & Mungal, M. G. (2004). Simultaneous measurements of scalar and velocity field evolution in turbulent crossflowing jets. *Journal of fluid mechanics*, *513*, 1–45. https://doi.org/10.1017/S0022112004009401

Suzuki, Y. J., & Koyaguchi, T. (2012). 3-D numerical simulations of eruption column collapse: Effects of vent size on pressure-balanced jet/plumes. *Journal of Volcanology and Geothermal Research*, *221–222*, 1–13. https://doi.org/10.1016/j.jvolgeores.2012.01.013

Suzuki, Y. J., & Koyaguchi, T. (2015). Effects of wind on entrainment efficiency in volcanic plumes. *Journal of Geophysical Research: Solid Earth*, *120*, 6122–6140. https://doi.org/10.1002/2015JB012208

Suzuki, Y. J., & Koyaguchi, T. (2015). Effects of wind on entrainment efficiency in volcanic plumes. *Journal of Geophysical Research: Solid Earth*, *120*, 6122–6140. https://doi.org/10.1002/2015JB012208

Thring, M. W. (1953). Combustion length of enclosed turbulent jet flames. In *4th symposium on combustion* (pp. 789–796). William and Wilkins. https://doi.org/10.1016/S0082-0784(53)80103-7

Turner, J. (1986). Turbulent entrainment: The development of the entrainment assumption, and its application to geophysical flows. *Journal of Fluid Mechanics*, *173*, 431–471. https://doi.org/10.1017/S0022112086001222

Van Eaton, A. R., Amigo, A., Bertin, D., Mastin, L. G., Giacosa, R. E., González, J., et al. (2016). Volcanic lightning and plume behavior reveal evolving hazards during the April 2015 eruption of Calbuco volcano, Chile. *Geophysical Research Letters*, *43*, 3563–3571. https://doi.org/10.1002/2016GL068076

Vernier, J., Fairlie, T. D., Deshler, T., Natarajan, M., Knepp, T., Foster, K., et al. (2016). In situ and space-based observations of the Kelud volcanic plume: The persistence of ash in the lower stratosphere. *Journal of Geophysical Research: Atmospheres*, *121*, 11,104–11,118. https://doi.org/10.1002/2016JD025344

Woodhouse, M. J., Hogg, A. J., Phillips, J. C., & Rougier, J. C. (2015). Uncertainty analysis of a model of wind-blown volcanic plumes. *Bulletin of Volcanology*, *77*(10), 83. https://doi.org/10.1007/s00445-015-0959-2

Woodhouse, M., Hogg, A., Phillips, J., & Sparks, R. (2013). Interaction between volcanic plumes and wind during the 2010 Eyjafjallajökull eruption, Iceland. *Journal of Geophysical Research: Solid Earth*, *118*, 92–109. https://doi.org/10.1029/2012JB009592

Woods, A. (1988). The fluid dynamics and thermodynamics of eruption columns. *Bulletin of Volcanology*, *50*(3), 169–193. https://doi.org/10.1007/BF01079681

Woods, A., & Bower, S. (1995). The decompression of volcanic jets in a crater during explosive volcanic eruptions. *Earth and Planetary Science Letters*, *131*(3-4), 189–205. https://doi.org/10.1016/0012-821X(95)00012-2

Woods, A., & Caulfield, C. (1992). A laboratory study of explosive volcanic eruptions. *Journal of Geophysical Research*, *97*(B5), 6699–6712. https://doi.org/10.1029/92JB00176